Journal of Microwaves, Optoelectronics and Electromagnetic Applications, Vol. 23, No. 3, e2024284768 Sep 2024
DOI: http://dx.doi.org/10.1590/2179-10742024v23i3284768

Article

Non-Uniform Phase Synthesis for Cosecant-Squared Radiation Patterns

Pedro A. B. Leão[1], Tcharles V. B. Faria[1], Fernando J. S. Moreira[2]
[1]*Graduate Program in Electrical Engineering, Federal University of Minas Gerais, Belo Horizonte, MG, 31270-901, Brazil, pedrobessaleao@ufmg.br, tcharlesdefaria@ufmg.br*
[2]*Department of Electronics Engineering, Federal University of Minas Gerais, Belo Horizonte, MG, 31270-901, Brazil, fernandomoreira@ufmg.br*

***Abstract*— In the present work an analytical formulation to synthesize non-uniform phase distributions at cylindrical apertures is described. Assuming three distinct amplitude distributions, the respective phases are established to provide cosecant-squared radiation patterns. Non-uniform amplitude distributions are investigated and adopted to reduce sidelobe levels and unwanted ripples in the synthesized radiation patterns. Analytical results for the established amplitude and phase distributions at cylindrical apertures are presented. The radiation patterns for such distributions are obtained by aperture method analysis, successfully demonstrating the usefulness of the new analytical formulation.**

***Index Terms*—** Omnidirectional aperture antennas, Cosecant-squared radiation pattern, Aperture method.

I. Introduction

Cosecant-squared radiation patterns may be an important option for mobile communication systems and air surveillance radar applications [1], [2]. Such radiation patterns compensate for propagation losses, providing greater directivity in the directions of longer pathways [3]. Fig. 1 shows an example of the idealized cosecant-squared radiation pattern, for directions between 105 and 155 degrees. Techniques for synthesizing amplitude and phase distributions at aperture antennas to provide cosecant-squared radiation patterns have been investigated for quite a long time [4]. In [4], for example, the authors employed the Stationary Phase Method (SPM) to propose a differential equation in order to determine the non-uniform phase distribution over a planar aperture to obtain the desired radiation pattern.

There are various types of antennas designed to meet the specifications of the cosecant-squared radiation pattern, as seen in [5] and [6]. In [5], an antenna array based on integrated substrate waveguide (SIW) technology for 5G base stations was investigated, emphasizing the importance of cosecant-squared radiation patterns in mobile networks. Additionally, there are studies that use optimization algorithms to attain the desired pattern [6].

Among the antennas that meet the specifications for radiating a cosecant-squared pattern, it is important to mention the omnidirectional dual-reflector configurations [1], [7], [8]. In these works, the shaping of the main-reflector was suited to generate a cosecant-squared radiation pattern in the elevation plane for a uniform coverage, but only controlling the far-field power density. It is known that the synthesis of both amplitude and phase distributions at the antenna aperture is a fundamental tool in the shaping of dual-reflector antennas for a more efficient radiation of the desired pattern.

Brazilian Microwave and Optoelectronics Society-SBMO *received 20 Mar 2024; for review 10 May 2024; accepted 01 Sep 2024*
Brazilian Society of Electromagnetism-SBMag *ISSN 2179-1074*

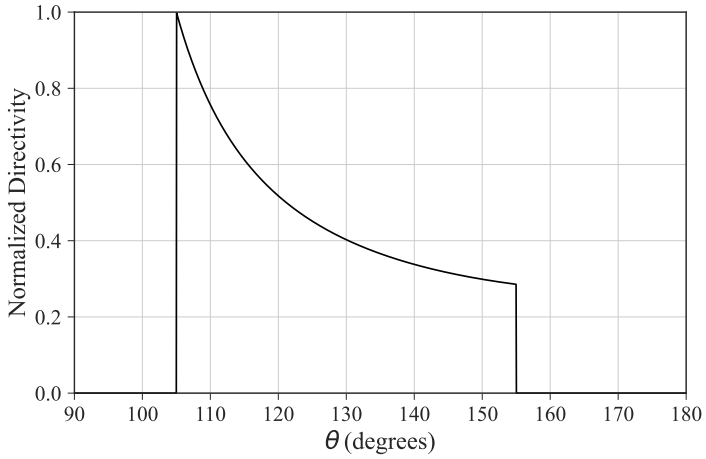

Fig. 1. Example of the desired cosecant-squared radiation pattern for directions between 105 and 155 degrees.

Continuing the studies of [4], in [9] a method was proposed to obtain a non-uniform phase distribution at planar apertures, adopting a constant amplitude. However, the resulting radiation patterns showed high sidelobe levels and unwanted ripples. This can be avoided by employing a tapered amplitude distribution at the aperture [10]. In [10], however, the phase at the antenna aperture is constant and can not provide a cosecant-squared pattern. Recently, in [11], an antenna design procedure was proposed in which the phase synthesis of [4] is achieved based on the tapered amplitude distribution at the aperture of the omnidirectional dual-reflector proposed in [10]. It should be noted that these omnidirectional antennas have cylindrical apertures. Thus, the present work, which is an extension of [11] and [12], investigates an antenna design procedure where the phase synthesis of [4] is obtained for new amplitude distributions in cylindrical apertures, which have not yet been explored in the literature.

This study is organized as follows. Section II presents the formulation for the phase synthesis at cylindrical apertures. The method is based on [9], but two different tapered amplitude distributions are considered to reduce sidelobe levels and ripples of the radiation pattern. Given the amplitude distributions at the aperture and the desired cosecant-squared pattern, the corresponding phase distributions are obtained, two of them in closed form (a significant contribution of this work). In Section III, the Aperture Method (Ap-M) equations are described and used to validate the phase synthesis technique. Relevant case studies are presented and discussed in Section IV. Finally, conclusions are presented in Section V.

II. Non-Uniform Phase Synthesis Technique

The synthesis technique for determining the non-uniform phase distribution $\psi(\xi)$ over the cylindrical aperture to provide the cosecant-squared radiation pattern is based on the theory of [9]. The steps of the present technique are schematically illustrated in Fig. 2. According to Fig. 2, note that two functions must be defined: $F_{norm}(u)$ and $G_A(\xi)$. The function $F_{norm}(u)$ represents the desired far field amplitude in the antenna elevation plane and $G_A(\xi)$ is the prescribed power density over the cylindrical aperture, proportional to the square of the aperture field amplitude (i. e., the amplitude is given by $\sqrt{G_A}$).

For a cosecant-squared radiation pattern, $F_{norm}(u)$ is expressed as follows [9]:

received 20 Mar 2024; for review 10 May 2024; accepted 01 Sep 2024

ISSN 2179-1074

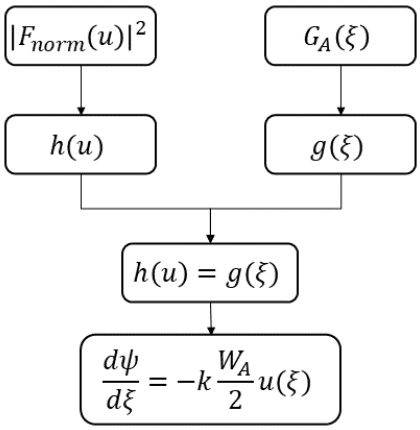

Fig. 2. Flowchart of the non-uniform phase synthesis technique.

$$F_{norm}(u) = \begin{cases} 0, & -1 \leq u \leq u_1 \\ A/u, & u_1 < u < u_2 \\ 0, & u_2 \leq u \leq 1 \end{cases}, \tag{1}$$

where $u = \sin(\theta - 3\pi/2)$ represents the direction of observation at the antenna far-field, $u_1 = \sin(\theta_1 - 3\pi/2)$, $u_2 = \sin(\theta_2 - 3\pi/2)$. Consequently, $\theta = 0°$ and $180°$ correspond to $u = -1$ and $+1$, respectively. The angles θ_1 and θ_2 define the starting and ending directions of the cosecant-squared radiation pattern, as illustrated in Fig. 3. From the definition of $F_{norm}(u)$ in (1), the normalized radiated power density is:

$$h(u) = \frac{\int_{-1}^{u} |F_{norm}(\tau)|^2 \, d\tau}{\int_{-1}^{1} |F_{norm}(\tau)|^2 \, d\tau}, \tag{2}$$

where τ is a dummy integration variable. Considering the desired cosecant-squared pattern for $\theta_1 < \theta < \theta_2$ given by (1), the normalized radiation power density in (2) is analytically evaluated as:

$$h(u) = \frac{u_2 \, (u - u_1)}{u \, (u_2 - u_1)}. \tag{3}$$

Furthermore, the normalized aperture power density $g(\xi)$ is defined by:

$$g(\xi) = \frac{\int_{-1}^{\xi} G_A(\eta) \, d\eta}{\int_{-1}^{1} G_A(\eta) \, d\eta}, \tag{4}$$

where ξ is the normalized cylindrical aperture coordinate along the axial direction, such that $\xi = -1$ at the bottom of the aperture and $\xi = 1$ at the top (see Fig. 3), and η is a dummy integration variable.

From $h(u)$ and $g(\xi)$ provided by equations (3) and (4), respectively, it is possible to obtain the mapping function $u(\xi)$ by directly imposing energy conservation:

$$h(u) = g(\xi). \tag{5}$$

Finally, the non-uniform phase distribution $\psi(\xi)$ over the cylindrical aperture is determined by the

received 20 Mar 2024; for review 10 May 2024; accepted 01 Sep 2024

ISSN 2179-1074

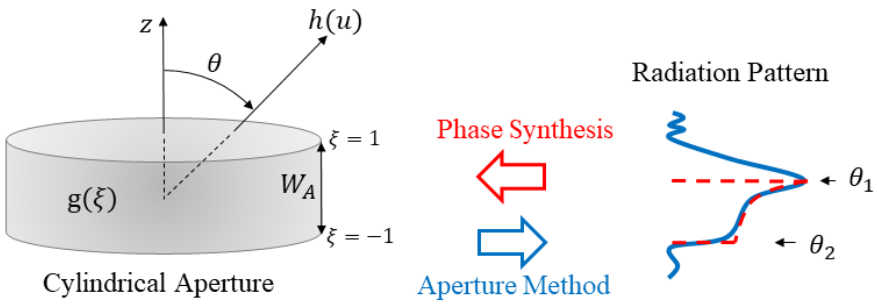

Fig. 3. Schematic representation of a cylindrical aperture for the cosecant-squared radiation pattern.

solution of the differential equation [9]:

$$\frac{d\psi(\xi)}{d\xi} = -k\frac{W_A}{2}u(\xi), \tag{6}$$

where $k = 2\pi/\lambda$ and W_A is the height of the cylindrical aperture (see Fig. 3). Depending of the complexity of $G_A(\xi)$, equations (4) and (6) may have to be evaluated numerically to determine the field distribution at a cylindrical aperture as a function of $\sqrt{G_A}$ (amplitude) and ψ (phase).

A. Analytical Solutions for Non-Uniform Phase

In the present study, we propose to obtain $\psi(\xi)$ adopting three different distributions for $G_A(\xi)$ (namely G_{A1}, G_{A2}, and G_{A3}). The investigated amplitude distributions are depicted in Fig. 4. Assuming $G_{A1} = 1$ for a cylindrical aperture, $g(\xi)$ is evaluated from (4) as [12]:

$$g(\xi) = \frac{1+\xi}{2}, \quad \text{for } -1 \leq \xi \leq 1. \tag{7}$$

Substituting (3) and (7) into (5), it is possible to obtain the mapping function $u(\xi)$ in analytical form:

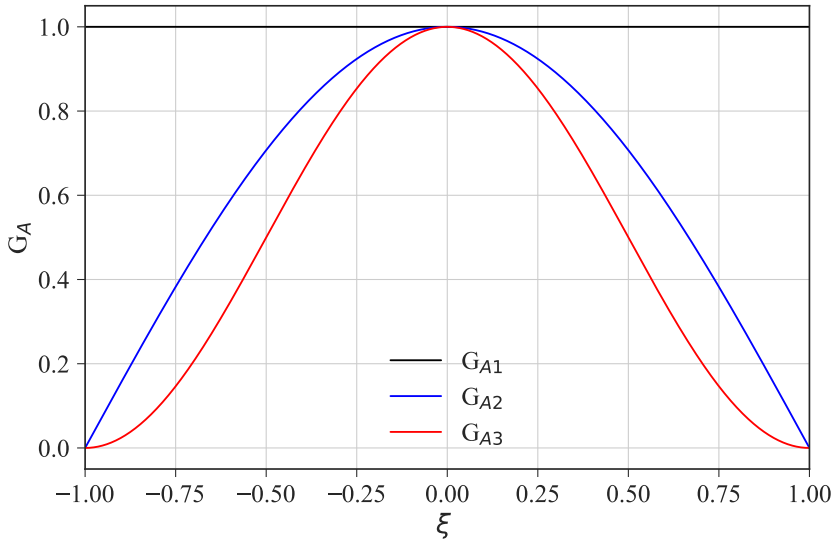

Fig. 4. Investigated G_A distributions.

received 20 Mar 2024; for review 10 May 2024; accepted 01 Sep 2024

ISSN 2179-1074

$$u(\xi) = \frac{2u_1u_2}{u_2 + u_1 - \xi(u_2 - u_1)}. \tag{8}$$

Evaluating (6) analytically with the help of (8), one obtains:

$$\psi(\xi) = \left(\frac{kW_A u_1 u_2}{u_2 - u_1}\right) \ln\left[u_2 + u_1 - \xi(u_2 - u_1)\right]. \tag{9}$$

However, the phase distribution given by equation (9) with uniform amplitude at aperture provides larger sidelobe levels [12]. To reduce these undesired sidelobe levels, we propose a tapered amplitude distribution (G_{A2}) that is given by (see Fig. 4):

$$G_{A2} = \cos\left(\frac{\xi\pi}{2}\right), \quad \text{for } -1 \leq \xi \leq 1. \tag{10}$$

Considering G_{A2} of (10), one can calculate the normalized power density $g(\xi)$ at a cylindrical aperture from (4):

$$g(\xi) = \frac{1 + \sin(\xi\,\pi/2)}{2}, \quad \text{for } -1 \leq \xi \leq 1. \tag{11}$$

From the conservation of energy, i.e. equating (3) to (11), one obtains:

$$u(\xi) = \frac{2\,u_1\,u_2}{2\,u_2 + [1 + \sin(\xi\,\pi/2)](u_1 - u_2)}. \tag{12}$$

Consequently, differential equation (6) is analytically evaluated to provide the following non-uniform phase distribution for G_{A2}:

$$\psi(\xi) = \frac{-2kW_A\sqrt{u_1}\sqrt{u_2}}{\pi}\ \tan^{-1}\left[\frac{(u_1 + u_2)\tan(\xi\,\pi/4) + u_1 - u_2}{2\sqrt{u_1}\sqrt{u_2}}\right]. \tag{13}$$

Extending the analysis, another possible amplitude distribution over the cylindrical aperture, with a more intense attenuation at the aperture edges than G_{A2}, is given by (see Fig. 4):

$$G_{A3} = \cos^2\left(\frac{\xi\pi}{2}\right), \quad \text{for } -1 \leq \xi \leq 1. \tag{14}$$

Following the same steps described to obtain the previous phases, the mapping function $u(\xi)$ for G_{A3} is given by:

$$u(\xi) = \frac{2\,u_1\,u_2}{2\,u_2 + [1 + \xi + \sin(\xi\,\pi)/\pi](u_1 - u_2)}. \tag{15}$$

Finally, given equation (15), the differential equation (6) must be numerically evaluated. Thus, the phase distribution $\psi(\xi)$ corresponding to the amplitude distribution G_{A3} must be numerically obtained.

III. Radiated Far-Field by the Aperture Method

In the present work, Ap-M is used to validate the non-uniform phase synthesis technique described in Sect. II. The amplitude ($\sqrt{G_A}$) and phase (ψ) distributions synthesized for the cylindrical aperture are then employed to establish the equivalent surface current densities, which are further integrated to

received 20 Mar 2024; for review 10 May 2024; accepted 01 Sep 2024

ISSN 2179-1074

determine the radiated far field [13]. According to the equivalence principle [14], the equivalent electric and magnetic current densities $\vec{J}_A(\vec{r}_A)$ and $\vec{M}_A(\vec{r}_A)$, respectively, are obtained:

$$\vec{J}_A(\vec{r}_A) = -\frac{[G_A(\xi)]^{1/2}\, e^{j\psi(\xi)}}{Z_0}\hat{z}, \tag{16}$$

$$\vec{M}_A(\vec{r}_A) = [G_A(\xi)]^{1/2}\, e^{j\psi(\xi)}\hat{\phi}, \tag{17}$$

where $Z_0 = \sqrt{\mu_0/\epsilon_0}$ is the free-space impedance.

From the radiation integral equation [13], the electric far field radiated by $\vec{J}_A(\vec{r}_A)$ and $\vec{M}_A(\vec{r}_A)$ is calculated:

$$\vec{E}(\vec{r}) \approx -j\frac{kZ_0}{4\pi}\frac{\exp(-jkr)}{r}\iint_{S_A}\left\{\vec{J}_A(\vec{r}\,') - \left[\vec{J}_A(\vec{r}\,')\cdot\hat{r}\right]\hat{r} + \frac{1}{Z_0}\vec{M}_A(\vec{r}\,')\times\hat{r}\right\}\exp(jk\vec{r}\,'\cdot\hat{r})\, dS_A, \tag{18}$$

where $\vec{r}\,'$ locates the equivalent currents at the aperture and dS_A is the infinitesimal cylindrical area given by

$$dS_A = \frac{W_A}{2}\,\rho_A\, d\xi'\, d\phi', \tag{19}$$

with ρ_A being the radius of the cylindrical aperture. The dot product $\vec{r}\,'\cdot\hat{r}$ in (18) can be evaluated as:

$$\vec{r}\,'\cdot\hat{r} = \rho_A\sin\theta\cos(\phi-\phi') + \frac{W_A}{2}\,\xi'\cos\theta. \tag{20}$$

Furthermore, using (16) and (17) with a proper coordinate conversion, one obtains:

$$\begin{aligned}\vec{J}_A(\vec{r}\,') \;-\; &\left[\vec{J}_A(\vec{r}\,')\cdot\hat{r}\right]\hat{r} \;+\; \frac{1}{Z_0}\vec{M}_A(\vec{r}\,')\times\hat{r} \\ &= \;\frac{1}{Z_0}\left\{\left[\sin\theta + \cos(\phi-\phi')\right]\hat{\theta} - \cos\theta\sin(\phi-\phi')\,\hat{\phi}\right\}\left[G_A(\xi')\right]^{1/2}\,\exp[j\psi(\xi')].\end{aligned} \tag{21}$$

Substituting (19)–(21) into (18), one obtains the spherical θ-component of the electric field in the far-field region, after integration over ϕ':

$$\begin{aligned}E_\theta(\vec{r}) \approx &-\frac{jkW_A\rho_A}{4}\frac{\exp(-jkr)}{r}\left[\sin\theta\,\mathrm{J}_0(k\rho_A\sin\theta) + j\mathrm{J}_1(k\rho_A\sin\theta)\right] \\ &\times\int_{-1}^{1}\left[G_A(\xi')\right]^{1/2}\exp[j(kW_A\xi'\cos\theta)/2]\;\exp[j\psi(\xi')]\,d\xi',\end{aligned} \tag{22}$$

where J_0 and J_1 are Bessel functions of order zero and one, respectively. Due to the symmetry of the cylindrical aperture, the azimuthal component of the electric field in the far-field region is zero (i. e., $E_\phi = 0$). Finally, the directivity can be calculated by:

$$D(\theta,\phi) = \frac{2\pi|rE_\theta(\vec{r})|^2}{Z_0 P_{rad}}, \tag{23}$$

where P_{rad} is the power radiated by the aperture, given by:

Brazilian Microwave and Optoelectronics Society-SBMO received 20 Mar 2024; for review 10 May 2024; accepted 01 Sep 2024
Brazilian Society of Electromagnetism-SBMag ISSN 2179-1074

$$P_{rad} = \frac{1}{2Z_0} \oiint |E_\theta(\vec{r})|^2 \, r^2 \, \text{sen}\theta \, d\theta \, d\phi. \tag{24}$$

Thus, (22) and (24) can be numerically evaluated using the SciPy library in the Python programming language [15].

IV. Case Studies

To demonstrate the usefulness of the synthesis technique proposed in this work, some case studies are presented considering the three non-uniform phase distributions obtained by G_{A1}, G_{A2}, and G_{A3}. For each case study, a comparison is established among the three phase distributions $\psi(\xi)$. The radiation patterns provided by such distributions were simulated by the Ap-M analysis of Sect. III. From the results presented, we evaluate the influence of the parameter W_A on the phase calculation and the corresponding radiation patterns. Afterwards, a variation of angle θ_2 is performed to verify whether the present synthesis technique meets the desired pattern beam-width specifications (see Fig. 3).

In the first case study, ψ is obtained for the three distributions G_{A1}, G_{A2}, and G_{A3} with $W_A = 10\lambda$, aiming for a cosecant-squared radiation pattern given by (1) with $\theta_1 = 95°$ and $\theta_2 = 140°$. Fig. 5 shows the three distributions $\psi(\xi)$ determined from (9) and (12) for G_{A1} and G_{A2}, respectively, and from the numerical evaluation of (6) for G_{A3}. The graphs are given in terms of the aperture coordinate z instead of ξ. From the figure one observes that the phase variation in the cylindrical aperture considering G_{A3} is greater than the others. Fig. 6 presents the cosecant-squared pattern defined by (1) for $\theta_1 < \theta < \theta_2$ and the Ap-M radiation patterns obtained for G_{A1}, G_{A2}, G_{A3}, and their respective phases $\psi(\xi)$. Due to the tapered behavior of (10) and (14) over the cylindrical aperture (i. e., for $-1 < \xi < 1$), G_{A2} and G_{A3} are both capable of reducing undesirable ripples in the radiation pattern for $95° < \theta < 140°$, as

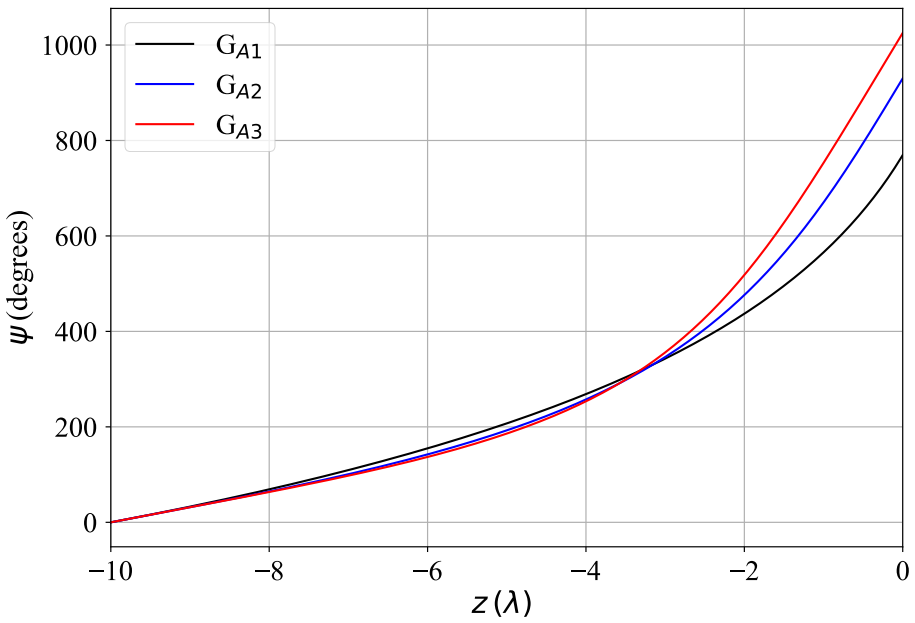

Fig. 5. Phase distributions ψ for G_{A1}, G_{A2}, and G_{A3} of the first case study.

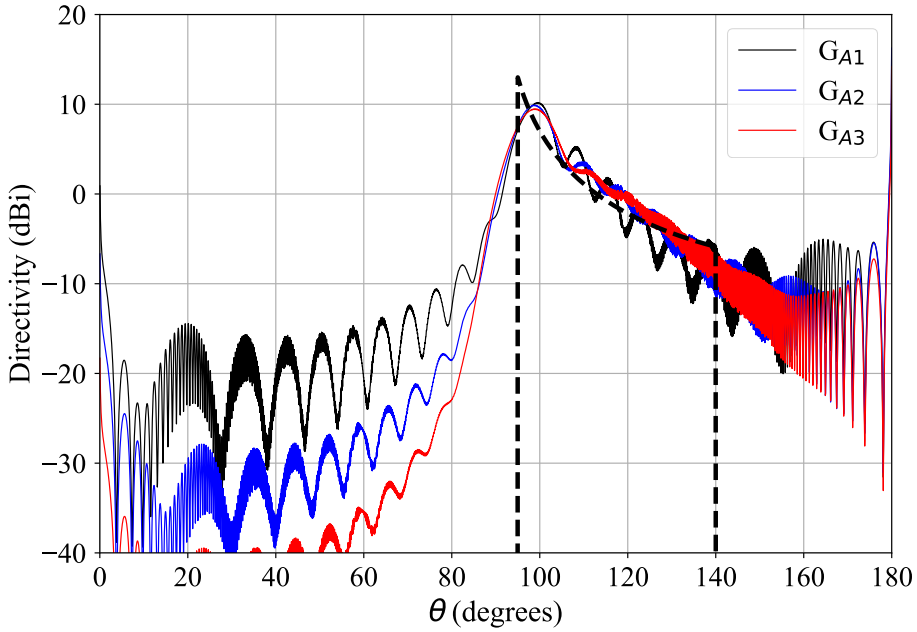

Fig. 6. Ap-M radiation patterns for the first case study.

desired. Particularly, the distribution G_{A3}, which has the most intense field attenuation at the aperture edges, provides the smallest sidelobe levels, as expected.

In the second case study, the values of θ_1 and θ_2 were kept equal to $95°$ and $140°$, respectively, but the width W_A of the cylindrical aperture was increased to 50λ. The phases ψ were calculated for G_{A1}, G_{A2}, and G_{A3} as in the first case, and are illustrated in Fig. 7. From this figure one observes that the

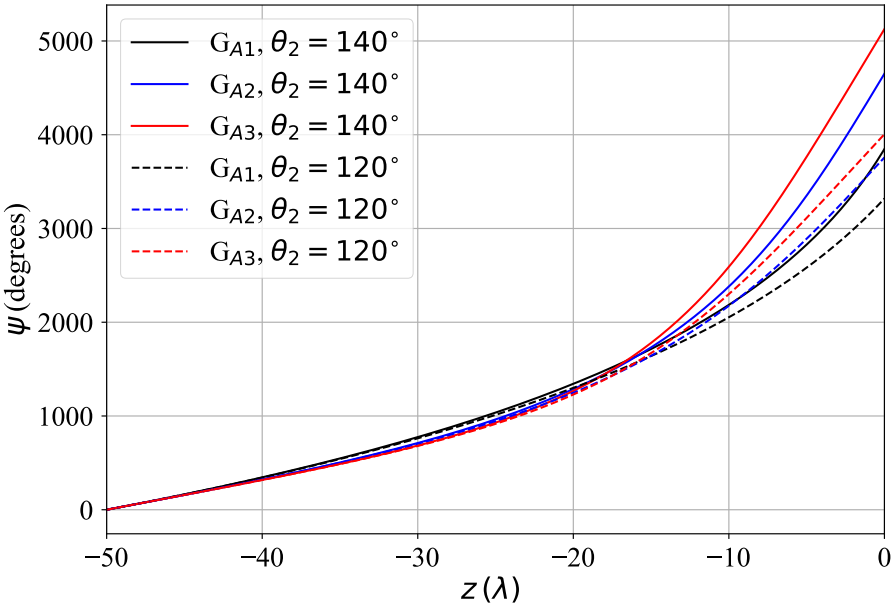

Fig. 7. Phase distributions ψ for G_{A1}, G_{A2}, and G_{A3} of the second and third case studies.

ISSN 2179-1074

phase distributions basically have the same behavior of those of the first case illustrated in Fig. 5. The Ap-M radiation patterns are illustrated in Fig. 8 with the corresponding cosecant-squared template. As expected, the increase of W_A from 10λ to 50λ provides better control of the power density radiated by the aperture and, consequently, the present radiation patterns have a better conformity with the desired cosecant-squared pattern than those for $W_A = 10\lambda$ illustrated in Fig. 6. Once again, note that for (10) and (14), the radiation patterns determined by the Ap-M show lower sidelobe levels than those of the uniform distribution G_{A1}.

The third case study was conducted for $\theta_2 = 120°$, keeping $\theta_1 = 95°$ and $W_A = 50\lambda$. The phase distributions for G_{A1}, G_{A2}, and G_{A3} are shown in Fig. 7 with dashed lines. It can be observed that, as in the previous cases, the phase related to G_{A1} shows a smaller variation, while the one for G_{A3} has a greater variation over the aperture. It is also noteworthy that, compared to the second case study (shown with solid lines in Fig. 7), the reduction of angle θ_2 from $140°$ to $120°$ led to a decrease in the phase variation over the aperture. The corresponding Ap-M radiation patterns are shown in Fig. 9, from which one observes that, once more, the three amplitude distributions provided radiation patterns conformed to the idealized cosecant-squared pattern. However, the tapered amplitude distributions G_{A2} and G_{A3} proposed in this work provide a considerable reduction of the sidelobe levels. Additionally, it is noteworthy that, among the non-uniform amplitude distributions, G_{A3} exhibited lower sidelobe levels and pattern ripples than G_{A2} and, obviously, G_{A1}.

The maximum directivity values obtained in Fig. 6, Fig. 8, and Fig. 9 for all three case studies are summarized in Table I. From the table one observes that, according to the Ap-M simulations, the uniform amplitude G_{A1} always provides the highest directivity, while G_{A3} always provides the smallest one. This exemplifies the compromise between higher directivities and lower sidelobe levels that the antenna designer must keep in mind, in which case the present formulation can be used as a useful design tool.

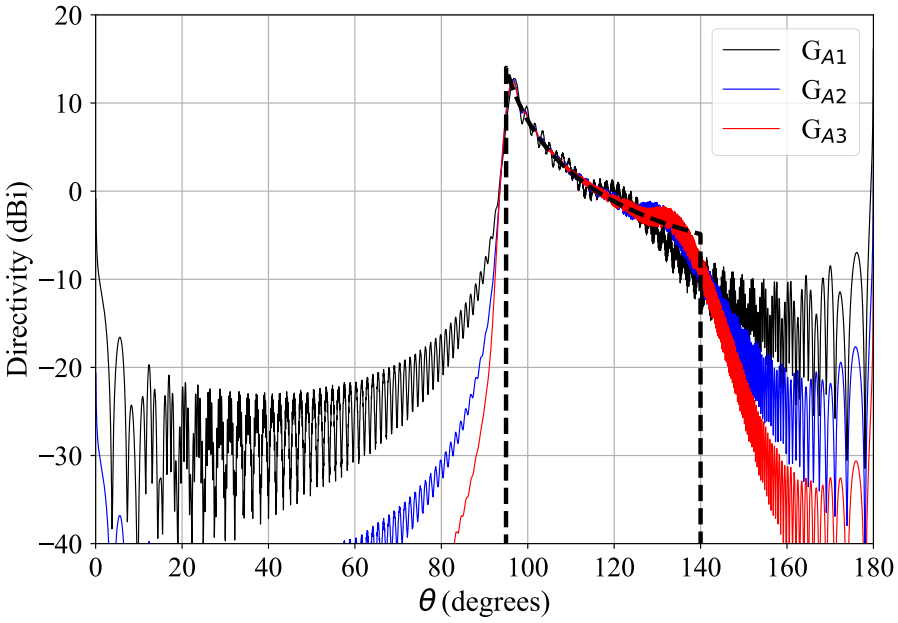

Fig. 8. Ap-M radiation patterns for the second case study.

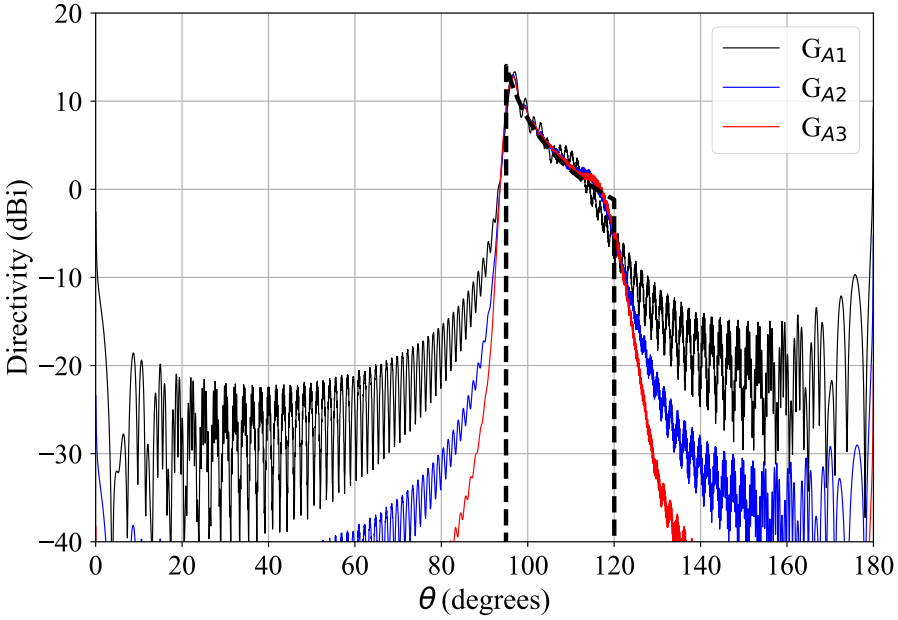

Fig. 9. Ap-M radiation patterns for the third case study.

TABLE I. Maximum directivity for the three investigated amplitude distributions G_A.

Case	Amplitude	Directivity (dBi)	θ (degrees)
1	G_{A1}	10.19	99.44
	G_{A2}	9.91	98.83
	G_{A3}	9.50	98.83
2	G_{A1}	12.78	96.75
	G_{A2}	12.68	96.65
	G_{A3}	12.41	96.65
3	G_{A1}	13.33	97.03
	G_{A2}	12.99	96.65
	G_{A3}	12.78	96.37

V. CONCLUSIONS

A technique for synthesizing non-uniform phase distributions over cylindrical apertures to provide cosecant-squared radiation patterns was described, incorporating three distinct amplitude distributions. One of them is uniform and the other two are tapered at the aperture edges to reduce sidelobe levels and undesired ripples in the antenna radiation pattern. The phase distributions obtained were validated by Ap-M analysis, confirming that the tapered amplitudes indeed reduce the sidelobe levels. It is also noteworthy that analytical solutions for non-uniform phase distributions were derived for the amplitude distributions G_{A1} and G_{A2}.

ACKNOWLEDGMENTS

This work was supported in part by CNPq (303257/2022-9), FAPEMIG (PPM-00384-18), and CAPES-PROEX, Brazil.

REFERENCES

[1] R. A. Penchel, J. R. Bergmann, and F. J. S. Moreira, "Main-reflector shaping of omnidirectional dual reflectors using local conic sections," *IEEE Transactions on Antennas and Propagation*, vol. 61, pp. 4379–4383, 2013.

[2] Z. C. Hao and M. He, "Developing millimeter-wave planar antenna with a cosecant squared pattern," *IEEE Transactions on Antennas and Propagation*, vol. 65, pp. 5565–5570, 2017.

[3] K. Q. Henderson and N. Ghalichechian, "Triangular and rectangular lattices for cosecant-squared-shaped beam reflectarrays," *IEEE Antennas and Wireless Propagation Letters*, vol. 20, pp. 2058–2062, 2021.

[4] A. K. Chakraborty, B. N. Das, and G. S. Sanyal, "Determination of phase functions for a desired one-dimensional pattern," *IEEE Transactions on Antennas and Propagation*, vol. 29, pp. 502–506, 1981.

[5] J. Puskely, T. Mikulasek, Y. Aslan, A. Roederer, and A. Yarovoy, "5G SIW-based phased antenna array with cosecant-squared shaped pattern," *IEEE Transactions on Antennas and Propagation*, vol. 70, pp. 250–259, 2022.

[6] D. Zhao, C. Bian, L. Wang, Z. Sun, R. Xie, P. Li, and Y. Rui, "Synthesis of cosecant squared pattern based on convex optimization," in *2019 International Applied Computational Electromagnetics Society Symposium - China (ACES), Nanjing, China*, pp. 1–2, 2019.

[7] L. Besso, R. Billis, R. Brachat, and R. Vallauri, "A milimetric wave omnidirectional antenna with cosecant squared elevation pattern," in *10th International Conference on Antennas and Propagation (ICAP 1997)*, pp. 448–451, 1997.

[8] J. R. Bergmann and F. J. S. Moreira, "Bandwidth behavior of omnidirectional dual-reflector antennas synthesized for uniform coverage," *Journal of Microwaves, Optoelectronics, and Electromagnetic Applications*, vol. 8, pp. S1–S8, 2009.

[9] M. Biswas, *An aperture synthesis technique for cylindrical printed lens/transmitarray antennas with shaped beams*. Master thesis, University of Ottawa, Canada, 2013.

[10] F. J. S. Moreira, A. Prata-Jr., and J. R. Bergmann, "GO shaping of omnidirectional dual-reflector antennas for a prescribed equi-phase aperture field distribution," *IEEE Transactions on Antennas and Propagation*, vol. 55, pp. 99–106, 2007.

[11] P. A. B. Leão, T. V. B. Faria, and F. J. S. Moreira, "Amplitude and phase synthesis at cylindrical apertures of omnidirectional dual-reflector antennas for uniform coverage," *IEEE Antennas and Wireless Propagation Letters*, vol. 23, pp. 2673–2677, 2024.

[12] ——, "Non-uniform phase synthesis for cosecant-squared radiation patterns," in *2023 SBMO/IEEE MTT-S International Microwave and Optoelectronics Conference (IMOC 2023)*, 2023.

[13] C. Balanis, *Antennas Theory: Analysis and Design*. New York: John Wiley and Son, 2016.

[14] R. F. Harrington, *Time-Harmonic Electromagnetic Fields*. New York: McGraw-Hill Book Co., 1961.

[15] P. Virtanen, R. Gommers, T. E. Oliphant, M. Haberland, T. Reddy, D. Cournapeau, E. Burovski, P. Peterson, W. Weckesser, J. Bright, S. J. van der Walt, M. Brett, J. Wilson, K. J. Millman, N. Mayorov, A. R. J. Nelson, E. Jones, R. Kern, E. Larson, C. J. Carey, İ. Polat, Y. Feng, E. W. Moore, J. VanderPlas, D. Laxalde, J. Perktold, R. Cimrman, I. Henriksen, E. A. Quintero, C. R. Harris, A. M. Archibald, A. H. Ribeiro, F. Pedregosa, P. van Mulbregt, and SciPy 1.0 Contributors, "SciPy 1.0: fundamental algorithms for scientific computing in Python," *Nature Methods*, vol. 17, pp. 261–272, 2020.

received 20 Mar 2024; for review 10 May 2024; accepted 01 Sep 2024

ISSN 2179-1074